

# Photomagnetic properties of iron(II) spin crossover complexes of 2,6-dipyrazolylpyridine and 2,6-dipyrazolylpyrazine ligands†

Chiara Carbonera,<sup>a</sup> José Sánchez Costa,<sup>a</sup> Victoria A. Money,<sup>b</sup> Jérôme Elhaïk,<sup>c</sup> Judith A. K. Howard,<sup>\*b</sup> Malcolm A. Halcrow<sup>\*c</sup> and Jean-François Létard<sup>\*a</sup>

Received 27th January 2006, Accepted 5th May 2006

First published as an Advance Article on the web 17th May 2006

DOI: 10.1039/b601366j

The photomagnetic properties of the following iron(II) complexes have been investigated:

[Fe(L<sup>1</sup>)<sub>2</sub>][BF<sub>4</sub>]<sub>2</sub> (**1**), [Fe(L<sup>2</sup>)<sub>2</sub>][BF<sub>4</sub>]<sub>2</sub> (**2**), [Fe(L<sup>3</sup>)<sub>2</sub>][ClO<sub>4</sub>]<sub>2</sub> (**3**), [Fe(L<sup>3</sup>)<sub>2</sub>][BF<sub>4</sub>]<sub>2</sub> (**4**), [Fe(L<sup>3</sup>)<sub>2</sub>][ClO<sub>4</sub>]<sub>2</sub> (**5**) and [Fe(L<sup>4</sup>)<sub>2</sub>][ClO<sub>4</sub>]<sub>2</sub> (**6**) (L<sup>1</sup> = 2,6-di{pyrazol-1-yl}pyridine; L<sup>2</sup> = 2,6-di{pyrazol-1-yl}pyrazine; L<sup>3</sup> = 2,6-di{pyrazol-1-yl}-4-{hydroxymethyl}pyridine; and L<sup>4</sup> = 2,6-di{4-methylpyrazol-1-yl}pyridine).

Compounds **1–6** display a complete thermal spin transition centred between 200–300 K, and undergo the light-induced excited spin state trapping (LIESST) effect at low temperatures. The *T*(LIESST) relaxation temperature of the photoinduced high-spin state for each compound has been determined.

The presence of sigmoidal kinetics in the HS → LS relaxation process, and the observation of LITH hysteresis loops under constant irradiation, demonstrate the cooperative nature of the spin transitions undergone by these materials. All the compounds in this study follow a previously proposed linear relation between *T*(LIESST) and their thermal spin-transition temperatures *T*<sub>1/2</sub>: *T*(LIESST) = *T*<sub>0</sub> – 0.3*T*<sub>1/2</sub>. *T*<sub>0</sub> for these compounds is identical to that found previously for another family of iron(II) complexes of a related tridentate ligand, the first time such a comparison has been made.

Crystallographic characterisation of the high- and low-spin forms of **5** and **6**, the light-induced high-spin state of **5**, and the low-spin complex [Fe(L<sup>4</sup>)<sub>2</sub>][BF<sub>4</sub>]<sub>2</sub> (**7**), are described.

## Introduction

One of the more fascinating examples of molecular bistability is the spin crossover (SCO) phenomenon encountered in some 3d<sup>4</sup>–3d<sup>7</sup> transition metal compounds.<sup>1</sup> Materials of this sort can switch reversibly between high- and low-spin electronic states in response to an external perturbation, such as a change in temperature or pressure, upon laser irradiation, or exposure to a strong magnetic field.<sup>2,3</sup> This phenomenon is consequently of particular interest, given the potential applications of spin-transition materials as molecular switches in information storage and display devices.<sup>4</sup> Spin-crossover effects are also important in some biological and geological systems.<sup>5</sup>

An increasingly important aspect of SCO research concerns the ability to control the colour or magnetic response of a molecular material photochemically. This represents a fascinating challenge, with clear applications in photonic devices. The photogeneration of long-lived metastable high-spin states in some iron(II) SCO materials is well-known, as the light-induced excited spin state trapping (LIESST) effect.<sup>6</sup> Several iron(II) compounds are known

to exhibit this effect, although in most cases the resultant metastable high-spin state is only long-lived at temperatures ≤50 K.<sup>7–9</sup> However, in some rare cases a photoinduced metastable state can be observed at 120 K.<sup>10</sup> Elucidation of the relation between the chemical structure of a LIESST compound, and the lifetime of its photogenerated excited state, will allow photoswitchable compounds operating at even higher temperatures to be designed.

In this context, we recently observed that three iron(II) complexes, [Fe(L<sup>1</sup>)<sub>2</sub>][BF<sub>4</sub>]<sub>2</sub> (**1**), [Fe(L<sup>2</sup>)<sub>2</sub>][BF<sub>4</sub>]<sub>2</sub> (**2**) and [Fe(L<sup>2</sup>)<sub>2</sub>][ClO<sub>4</sub>]<sub>2</sub> (**3**) (L<sup>1</sup> = 2,6-di{pyrazol-1-yl}pyridine; L<sup>2</sup> = 2,6-di{pyrazol-1-yl}pyrazine) also display long lifetimes for their photoinduced HS states, that are stable below the thermal relaxation temperatures [*T*(LIESST)<sup>11</sup>] of 80–100 K.<sup>12</sup> As a continuation of this work, we report here a full study of the photomagnetic properties of these and three other iron(II) complexes [Fe(L<sup>3</sup>)<sub>2</sub>][BF<sub>4</sub>]<sub>2</sub> (**4**), [Fe(L<sup>3</sup>)<sub>2</sub>][ClO<sub>4</sub>]<sub>2</sub> (**5**) and [Fe(L<sup>4</sup>)<sub>2</sub>][ClO<sub>4</sub>]<sub>2</sub> (**6**) (L<sup>3</sup> = 2,6-di{pyrazol-1-yl}-4-{hydroxymethyl}pyridine and L<sup>4</sup> = 2,6-di{4-methylpyrazol-1-yl}pyridine). Our data will be discussed in terms of the recently reported empirical linear relation between the thermal spin-transition temperature (*T*<sub>1/2</sub>), and the thermal stability of the photochemically generated high-spin state (*T*(LIESST), eqn (1)).<sup>9</sup>

$$T(\text{LIESST}) = T_0 - 0.3T_{1/2} \quad (1)$$

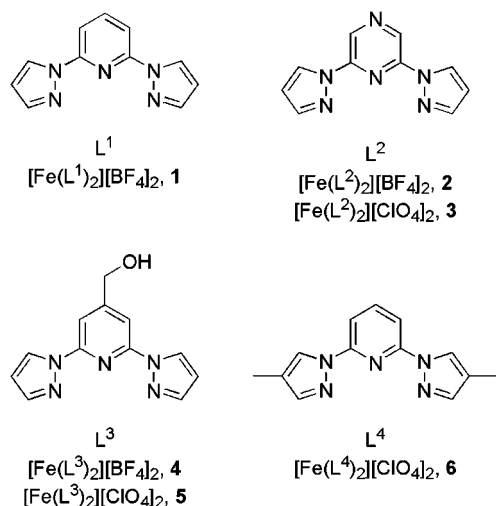
In particular, our results provide support for the observation that the intercept of this line, *T*<sub>0</sub>, varies in an apparently consistent way between different classes of compound. We also present detailed X-ray diffraction studies of the structural basis of spin crossover in the new compounds **5** and **6**.

<sup>a</sup>Institut de Chimie de la Matière Condensée de Bordeaux, UPR CNRS 9048-Université de Bordeaux 1, Groupe des Sciences Moléculaires, 87 Av. Doc. A. Schweitzer, F-33608, Pessac, France. E-mail: letard@icmcb-bordeaux.cnrs.fr

<sup>b</sup>Department of Chemistry, University of Durham, South Road, Durham, UK DH1 3LE. E-mail: j.a.k.howard@durham.ac.uk

<sup>c</sup>School of Chemistry, University of Leeds, Woodhouse Lane, Leeds, UK. LS2 9JT. E-mail: m.a.halcrow@leeds.ac.uk

† Electronic supplementary information (ESI) available: Additional details of the crystal structure of the low-spin complex salt [Fe(L<sup>4</sup>)<sub>2</sub>][BF<sub>4</sub>]<sub>2</sub> (**7**). See DOI: 10.1039/b601366j



## Results and discussion

The synthesis, thermal magnetochemistry and structural characterisation of **1**,<sup>12–14</sup> **2** and **3**,<sup>12,15</sup> and **4**,<sup>16</sup> have reported previously. Compound **5** is a new salt of the same complex dication as in **4**, with which it is isostructural. The new ligand  $L^4$  was synthesised by treatment of 2,6-dibromopyridine with 2.3 equiv. of potassium 4-methylpyrazolide following the usual procedure.<sup>17</sup> Complexation of  $\text{Fe}[\text{ClO}_4]_2 \cdot 6\text{H}_2\text{O}$  by two equiv. of  $L^4$  in acetone yielded **6** as mustard yellow microcrystals. A similar reaction using  $\text{Fe}[\text{BF}_4]_2 \cdot 6\text{H}_2\text{O}$  afforded the salt  $[\text{Fe}(L^4)_2][\text{BF}_4]_2$  (**7**), which is low-spin at room temperature.

### Magnetic and photomagnetic measurements

The temperature dependence of the magnetic susceptibility for **1–6** is shown in Fig. 1, and relevant data from these curves are collected in Table 1. Interestingly, all six complexes exhibit a thermal spin crossover with a complete conversion. At 290 K,  $\chi_M T$  for **1–3**

is ca.  $3.5 \text{ cm}^3 \text{ K mol}^{-1}$ , showing that these compounds exhibit a fully occupied quintet, high-spin state at room temperature. As previously described, these three compounds all show a complete and abrupt spin-transition upon cooling, with a small but reproducible hysteresis loop of 3–4 K. The behaviour of **6** is similar, showing an abrupt spin-transition at 233 K with 3 K hysteresis. However, its lower room-temperature  $\chi_M T$  value of  $2.8 \text{ cm}^3 \text{ K mol}^{-1}$  implies that the sample is heterogeneous, with ca. 20% being low-spin at room temperature. This is addressed further below. Finally, **4** and **5** show complete but more gradual spin-transitions, without hysteresis, with mid-points very close to room temperature. In all cases,  $\chi_M T$  below the spin transitions is close to  $0 \text{ cm}^3 \text{ K mol}^{-1}$ , as expected for a fully populated low-spin state ground state.

Thermal spin-crossover can be also monitored by following the visible spectrum of the sample as a function of the temperature, measured by diffuse reflectance. Fig. 2 shows the spectral changes for two of the compounds measured along their thermal spin transition. The band at 800–850 nm corresponds to a d–d transition of the high-spin iron(II) centre, while the absorptions in the 500–650 nm region can be assigned to both d–d and MLCT transitions of the low-spin material. Consequently, any change of the signal can be used to directly monitor the thermal SCO transition at the surface of the sample.<sup>18</sup> Hence, the increase of the reflectivity signal recorded at 650 nm for **4** and at 610 nm for **5** upon cooling (Fig. 2 inset) corresponds to the increasing population of the low-spin state following thermal SCO. The same reflectivity experiment can also monitor any light-induced phenomena occurring at the surface of the sample. When the temperature is sufficiently low that relaxation of the photoinduced high-spin state is slow, the light intensity at the surface of the sample can be used to tune the spin-state of the complex. In this sense, the reflectivity signal, which decreases along the thermal spin transition, reversely increases at lowest temperature (Fig. 2).

The low  $\rightarrow$  high spin photoconversion can be also investigated using a SQUID magnetometer coupled to an optical

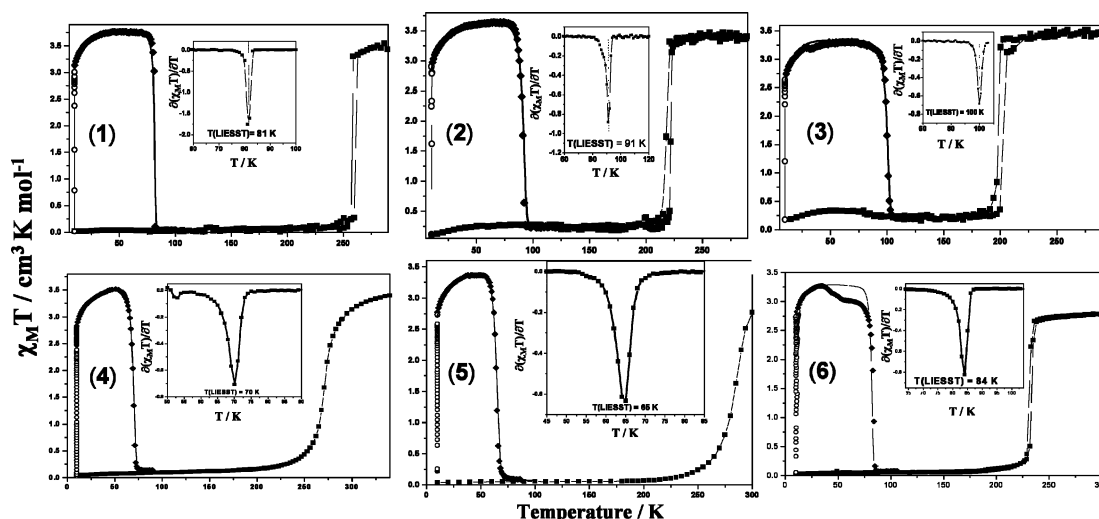


**Fig. 1** Temperature dependence of  $\chi_M T$  for **1–6**. ■ = data recorded in cooling and warming modes without irradiation; ○ = data recorded with irradiation at 10 K; ◆ =  $T(\text{LIESST})$  measurement, data recorded in warming mode with the laser turned off after irradiation for one hour. The solid line through the  $T(\text{LIESST})$  measurement shows the fit generated from the deduced experimental thermodynamic parameters. The insets show the derivate of the  $d\chi_M T/dT$  curves, whose minimum corresponds to  $T(\text{LIESST})$ .

**Table 1** Magnetic and photomagnetic properties of the compounds in this study<sup>a</sup>

	$T_{1/2}\downarrow$ /K	$T_{1/2}\uparrow$ /K	$T(\text{LIESST})$ /K	$T(\text{LITH})\downarrow$ /K	$T(\text{LITH})\uparrow$ /K
<b>1</b>	258	261	81	60	88
<b>2</b>	218	221	91	88	99
<b>3</b>	199	203	100	74	105
<b>4</b>	271	271	70	51	71
<b>5</b>	284	284	65	48	65
<b>6</b>	231	234	84	40	85

<sup>a</sup>  $T_{1/2}\downarrow$  and  $T_{1/2}\uparrow$  are the temperatures at which the sample contains 50% of LS and HS spins in the cooling and warming modes.  $T(\text{LIESST})$  is the temperature at which the light-induced HS information was erased in the SQUID cavity.  $T(\text{LITH})\uparrow$  and  $T(\text{LITH})\downarrow$  are the temperatures where there is apparently 50% of photoconverted HS molecules in cooling and warming modes under continuous irradiation.

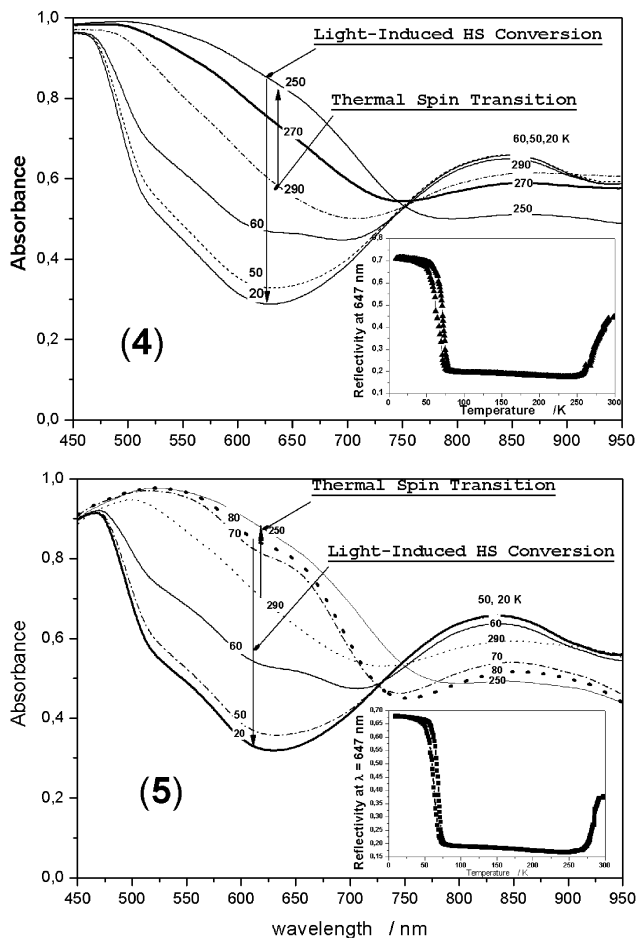


**Fig. 2** Changes in the reflectivity spectra of **4** and **5** upon cooling, and upon laser irradiation. The inset graphs show the intensity of the absorbance at 650 nm under the same conditions.

source.<sup>7-9,11,12,18</sup> For all of **1–6**, a drastic increase of the magnetic signal under light irradiation was observed at 10 K. The limit reached at photosaturation, after typically 1–2 hours of irradiation, was close to  $3.0 \text{ cm}^3 \text{ K mol}^{-1}$ . Fig. 1 shows the  $T(\text{LIESST})$  curve recorded for each compound. In this procedure, the irradiation is maintained until the signal is saturated, then the light is switched off and the temperature slightly increased at  $0.3 \text{ K min}^{-1}$ .<sup>7-9,11,19</sup> The minimum of the  $d\chi_M T/dT$  vs.  $T$  curve defines the limiting temperature  $T(\text{LIESST})$ , above which the light-induced magnetic high-spin information is erased in a SQUID cavity.<sup>11</sup>

The shapes of all the  $T(\text{LIESST})$  curves are almost identical. The  $\chi_M T$  product firstly increases upon warming from 10 K due to zero-field splitting of the high spin iron(II) ion, reaching a plateau of  $ca. 3.5 \text{ cm}^3 \text{ K mol}^{-1}$  near 20 K. For all of **1–6**,  $\chi_M T$  at the maximum of the  $T(\text{LIESST})$  curve is always close to the value recorded at room temperature. This confirms that for all these derivatives, light irradiation induces a 100% complete low  $\rightarrow$  high spin photoconversion, according to the light-induced excited spin state trapping effect. The  $T(\text{LIESST})$  values of **1–6** are collected in Table 1. As expected, the highest  $T(\text{LIESST})$  temperature is found for **3**, which exhibits the lowest thermal spin transition temperature ( $T_{1/2}$ ), in agreement with the inverse energy gap law introduced by Hauser *et al.*<sup>20</sup> Compound **6** consistently displays an anomaly upon rewarming, where a fraction of the sample undergoes LIESST relaxation at lower temperature than the bulk (Fig. 1). This is discussed further below.

The sharpness of the  $d\chi_M T/dT$  vs.  $T$  minima (Fig. 1 inset) for **1–6** implies that intermolecular cooperativity may play a role in thermal relaxation of their photogenerated high-spin excited states.<sup>19</sup> When the relaxation process follows simple stretched exponential behaviour, as encountered in non-cooperative SCO systems,<sup>21</sup> the minimum of the  $d\chi_M T/dT$  vs.  $T$  curve is not so well-defined.<sup>19</sup> We have therefore investigated the LIESST relaxation kinetics of **1–6**, at different temperatures between 10 K and the highest temperatures accessible with our SQUID set up, which are close to the  $T(\text{LIESST})$  values (Fig. 3). The strong deviation of these relaxation curves from a single exponential is striking, and they can be modelled using a sigmoidal law, consistent with the self-accelerated behaviour predicted for strong cooperative systems. This cooperativity arises from the large difference in metal–ligand bond lengths between high-spin and low-spin states, resulting in elastic interactions caused by the change in internal pressure inside the solids as the spin transition proceeds.<sup>18</sup> Thus, the height of the activation barrier to LIESST relaxation changes as a function of  $\gamma_{\text{HS}}$  (the fraction of spin centres in the sample that are high-spin at a given temperature), and the relaxation rate  $k_{\text{HL}}^*(T, \gamma_{\text{HS}})$  depends exponentially on both  $\gamma_{\text{HS}}$  and  $T$  (eqn (2) and (3)), where  $a(T)$  ( $=E_a^*/k_B T$ ) is the acceleration factor at a given temperature.

$$\frac{\partial \gamma_{\text{HS}}}{\partial T} = -k_{\text{HL}}^* \gamma_{\text{HS}} \quad (2)$$

$$k_{\text{HL}}^*(T, \gamma_{\text{HS}}) = k_{\text{HL}}(T) \exp[a(T)(1 - \gamma_{\text{HS}})] \quad (3)$$

Least squares fits of the data for **1–6** were performed using a sigmoidal model where  $k_{\text{HL}}(T)$  and  $a(T)$  were refined as free

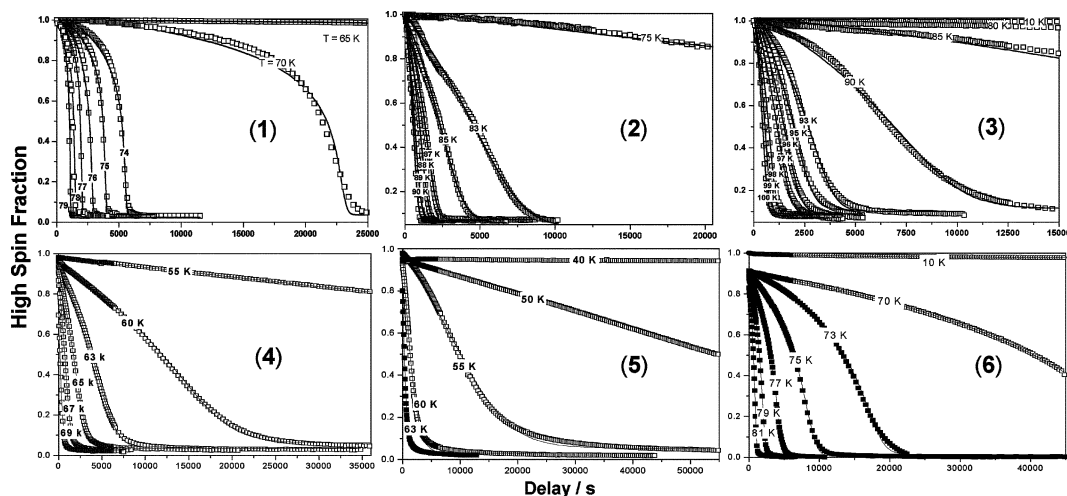


**Fig. 3** Time dependence at various temperatures of the high spin molar fraction generated by light irradiation at 10 K. Each point represents the high-spin fraction deduced from the magnetic response measured within the SQUID magnetometer around 30 s. The relaxation curves are fitted according to sigmoidal behaviour (Table 2).

**Table 2** Thermodynamic parameters for thermal relaxation from the LIESST high-spin state, where  $k_0$  is the overestimated limit of the tunnelling rate constant,  $k_\infty$  and  $E_a$  are respectively the pre-exponential factor and the activation energy of the activated region, and  $E_a^*$  the additional activation energy resulting from cooperativity

	$k_0/s^{-1}$	$k_\infty/s^{-1}$	$E_a/cm^{-1}$	$E_a^*/cm^{-1}$
1	$<7 \times 10^{-6}$	$8.0 \times 10^6$	1350	340–390
2	$8 \times 10^{-5}$	$9.3 \times 10^4$	1191	140–180
3	$<4.4 \times 10^{-5}$	$7.9 \times 10^7$	1770	180–200
4	$2 \times 10^{-6}$	$2.5 \times 10^9$	1350	120–130
5	$<4 \times 10^{-5}$	$4.4 \times 10^7$	1060	40–70
6	$1 \times 10^{-5}$	$5.1 \times 10^9$	1720	200–230

parameters. The calculated curves are shown as solid lines in Fig. 3, and the fitted parameters are listed in Table 2. The apparent activation energy,  $E_a$ , and the apparent pre-exponential factor,  $k_\infty$ , of the activated region are calculated from the straight line given by plotting  $\ln k_{HL}(T)$  vs.  $1/T$ .

An elegant way to test the validity of this model is to use the fitted parameters to reproduce the experimental  $T(LIESST)$  curve.<sup>19</sup> For that it is necessary to carefully take into account the time and temperature dependences. The main difficulty of this simulation is to satisfactorily estimate the rate constant  $k_0$  [i.e.  $k_{HL}(T \rightarrow 0)$ ], for relaxation by quantum mechanical tunnelling. For this, we consider that the last complete kinetic measurement recorded at low temperature can be regarded as an upper limit for the  $k_0$  value (Table 2). Based on this, and by using the deduced  $E_a$ ,  $k_\infty$  and  $\alpha(T)$  parameters, the agreement between the calculated and the experimental  $T(LIESST)$  curves was very good (Fig. 1).

Another way to measure the effect of cooperativity on the photoexcitation and subsequent relaxation processes is to monitor the magnetic properties of a spin crossover material under constant irradiation. Competition between the constant photoexcitation and self-accelerated thermal relaxation processes induces a thermal hysteresis loop near  $T(LIESST)$ , which is termed light-induced thermal hysteresis (LITH).<sup>11,22</sup> Fig. 4 and Table 1 show

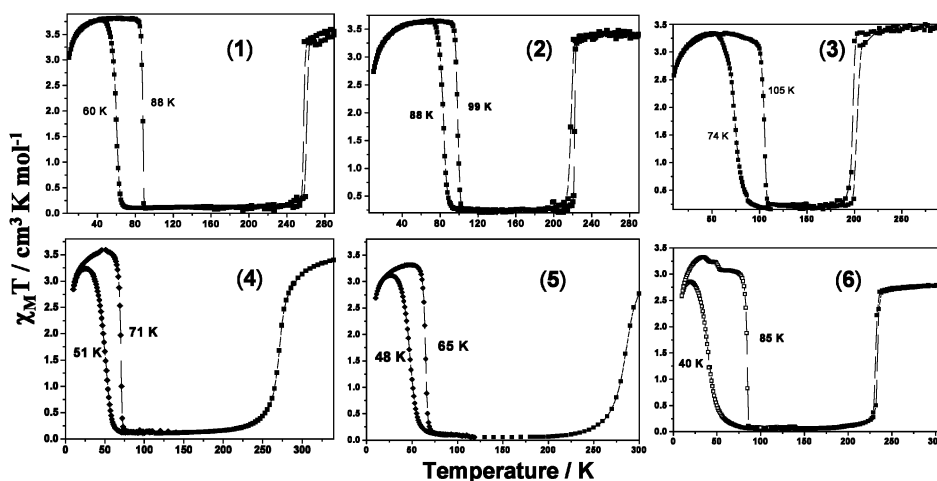


**Fig. 4** The temperature dependence of  $\chi_M T$  for 1–6 measured in warming and cooling modes under constant irradiation, showing their light-induced thermal hysteresis (LITH) properties. The LITH data from these graphs are listed in Table 1.

the LITH loops observed for **1–6** under constant irradiation. From these data it is also clear that the photo-induced high spin phase is characterised by a certain degree of cooperativity. There is only moderate correlation between the activation energy component arising from cooperativity in the samples ( $E_a^*$ , Table 2), which follows the trend:

$$5 < 4 < 2 < 3 < 6 < 1$$

and the magnitude of LITH hysteresis (Table 1):

$$2 < 4 < 5 < 1 \approx 3 < 6$$

However, it is notable that **4** and **5**, which exhibit the least cooperative thermal spin-transitions, also show the smallest  $E_a^*$  values and, with one exception, the narrowest LITH loops.

### Crystallography

A variable temperature crystallographic study of **5** has shown that it is isostructural with the previously described  $\text{BF}_4^-$  salt, **4**.<sup>16</sup> The compound crystallises in the monoclinic space group  $Cc$ ; the iron atom occupies a distorted octahedral environment and no crystallographic phase transition is found over the temperature of the experiment, selected crystallographic parameters are presented in Table 3. The hydroxyl groups of the ligands are found to be thermally disordered at 340 K. However, this disorder is resolved on cooling to 120 K and appears to play no role in determining the course of the spin transition. It was possible to refine anisotropic temperature factors for **5** only for the data collected at 340 K either due to crystal damage during the spin transition or the intrinsically poor quality of the crystals. The spin transition in this compound lies around ambient temperature, the same temperature at which crystallisation was performed, and this is the probable reason for the poor crystal quality. Iron–nitrogen bond lengths at 340 K, are diagnostic for high-spin iron(II), Table 4, on cooling to 30 K there is a decrease in the mean metal–ligand bond length of 0.180 Å, indicative of a spin transition from the high- to the low-spin state taking place between these two temperatures. Monitoring of the unit cell parameters with temperature, between 340 K and 30 K, demonstrates good agreement with the magnetic data with a sudden decrease in unit cell volume of 1.7% between 290 K and 270 K, clearly much greater than would be expected due to thermal contraction alone. These data show that there is little anisotropy, the  $a$  and  $b$  unit cell parameters decreasing by 0.5% between 290 K and 270 K while the  $c$  parameter decreases by 1% over the same temperature range. The  $\beta$  angle increases by 0.06%. The reduction in metal–ligand bond lengths on going from the high- to the low-spin state results in an increase in ligand bite angle. In common with the majority of spin crossover compounds, the low-spin state has a closer to ideal geometry than the high-spin state, as demonstrated by the lower values of the  $\Sigma$  and  $\nu$  parameters, as defined by Guionneau *et al.*<sup>23</sup>

Irradiation of the crystal in the low spin state at 30 K with red laser light ( $\lambda = 632.8$  nm, 25 mW) results in a transition to the metastable high-spin state, initial evidence for the transition is provided by the colour change of the crystal from brown to yellow. Full structural analysis reveals that after irradiation **5** is fully in the metastable high-spin state. It was not possible to refine anisotropic temperature factors for **5**, however the results are sufficiently accurate to allow differentiation of the high- and

**Table 3** Selected crystallographic parameters for the new compounds in this study

Compound	<b>5</b>	<b>5</b>	<b>5</b>	<b>6</b>	<b>6</b>	<b>6</b>	<b>7-0.2H<sub>2</sub>O</b>
Empirical formula	$\text{C}_{24}\text{H}_{32}\text{Cl}_2\text{FeN}_6\text{O}_{10}$	$\text{C}_{24}\text{H}_{32}\text{Cl}_2\text{FeN}_6\text{O}_{10}$	$\text{C}_{24}\text{H}_{32}\text{Cl}_2\text{FeN}_6\text{O}_{10}$	$\text{C}_{24}\text{H}_{36}\text{Cl}_2\text{FeN}_6\text{O}_8$	$\text{C}_{26}\text{H}_{36}\text{Cl}_2\text{FeN}_{10}\text{O}_8$	$\text{C}_{26}\text{H}_{36}\text{Cl}_2\text{FeN}_{10}\text{O}_8$	$\text{C}_{26}\text{H}_{36.4}\text{B}_2\text{F}_8\text{FeN}_{10}\text{O}_{0.2}$
Formula weight	737.27	737.27	737.27	737.27	733.32	733.32	711.64
Temperature/K	340	30	30	250	30	30	150
Spin state	High spin	Low spin	High spin	High spin	Low spin	Low spin	Low spin
Crystal system	Monoclinic	Monoclinic	Monoclinic	Tetragonal	Orthorhombic	Orthorhombic	Monoclinic
Space group	$Cc$	$Cc$	$Cc$	$P4_2/c$	$P2_1(2)_1$	$P2_1(2)_1$	$C2/c$
$a/\text{Å}$	12.269(3)	12.027(2)	12.052(2)	9.587(1)	9.600(2)	9.600(2)	30.5415(9)
$b/\text{Å}$	12.216(2)	12.038(2)	12.043(2)	17.933(4)	9.625(2)	9.625(2)	16.5009(6)
$c/\text{Å}$	20.572(4)	20.184(4)	20.105(4)	1648.1(5)	33.470(7)	33.470(7)	13.4070(5)
$\beta/^\circ$	99.61(3)	99.90(3)	98.66(3)	2	2	2	115.7118(15)
Volume/Å <sup>3</sup>	3040(1)	2878(1)	2884(1)	2	4	4	6087.6(4)
$Z$	4	4	4	2	4	4	8
$D_c/\text{Mg m}^{-3}$	1.611	1.701	1.697	1.478	1.575	1.575	1.553
$\mu/\text{mm}^{-1}$	0.744	0.786	0.784	0.682	0.727	0.727	0.583
Crystal size/mm	$0.22 \times 0.18 \times 0.18$	$0.22 \times 0.18 \times 0.18$	$0.22 \times 0.18 \times 0.18$	$0.18 \times 0.12 \times 0.08$	$0.18 \times 0.12 \times 0.08$	$0.18 \times 0.12 \times 0.08$	$0.27 \times 0.24 \times 0.22$
$\theta$ range/ $^\circ$	2.01 to 27.46	2.50 to 27.50	2.51 to 27.47	2.27 to 27.42	2.27 to 27.42	2.20 to 27.48	2.45 to 26.74
Reflections collected	9681	6091	6507	11139	16491	16491	24742
Independent reflections	5388	4122	4353	1893	6915	6915	6439
$R_{\text{int}}$	0.0632	0.0812	0.0700	0.0756	0.0998	0.0998	0.0879
$wR(F^2)$ (all data)	0.2367	0.3700	0.3200	0.2192	0.3182	0.3182	0.1529
$R(F)$ (all data)	0.1260	0.1602	0.1344	0.1149	0.1440	0.1440	0.1262
Refined parameters	437	192	192	115	194	194	454
GOF	1.019	1.170	1.184	1.041	1.125	1.125	0.989
$\Delta\rho_{\text{min,max}}/e \text{ Å}^{-3}$	0.86 and $-1.30$	4.01 and $-3.22$	3.87 and $-4.58$	1.00 and $-0.38$	3.47 and $-1.59$	3.47 and $-1.59$	0.62 and $-0.94$

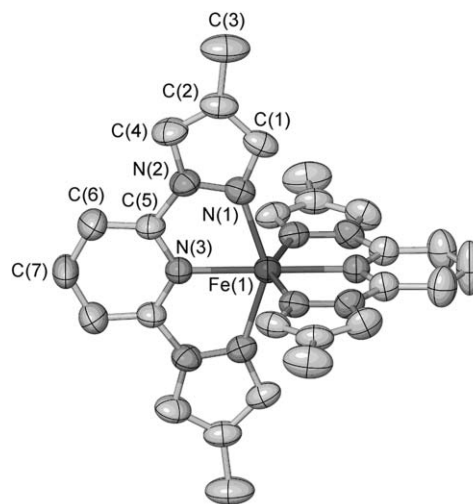
**Table 4** Selected geometrical parameters for **5** and **6**

	<i>T</i> /K	Mean Fe–N/Å	Bite angle/°	$\Sigma$ /°	<i>v</i> (%)
<b>5</b>	340	2.153(8)	74.0(3)	147.7	7.920
	30	1.97(1)	79.2(4)	94.0	3.750
	30	2.150(6)	73.8(2)	146.4	7.895
<b>6</b>	250	2.149(8)	72.7(2)	158.8	8.90
	30	1.947(9)	79.8(4)	96.3	3.44

low-spin states from examination of the metal–ligand bond lengths. The metal–ligand bond lengths after irradiation are diagnostic of an iron(II) centre in the high-spin state Table 4 increasing by 0.168 Å. The  $\Sigma$  parameters are the same for both the HS-1 and HS-2 indicating that complete conversion to the metastable high-spin state has been achieved. The increase in unit cell volume on irradiation is equal to 1.6%; very similar to that observed for the thermal spin transition. Of the previously reported metastable high-spin state structures two show significantly smaller increases in unit cell volume for the light induced transition than for the thermal spin transition.<sup>24</sup> A study of **1**<sup>14</sup> and the previously communicated results for **4**<sup>16</sup> showed that the difference in volume induced by irradiation with laser light was the same as that seen on going through the thermal spin transition. That the change in volume is the same on going through the thermal and light induced transitions is likely a result of the, comparatively, high packing density of this family of materials this also accounts for the comparatively small effect that cooling has on the volume of the systems. This point is particularly pertinent when it is considered that the changes observed in both earlier studies, concern the conformation of the monodentate NCS<sup>−</sup> or NCSe<sup>−</sup> ligands.

The addition of a CH<sub>2</sub>OH group to the **4** position of the central pyridine ring of the 2,6-dipyrazol-1-yl-pyridine ligand allows the formation of some weak hydrogen bonds, but in comparison with **1**,<sup>14</sup> and the BF<sub>4</sub> and ClO<sub>4</sub> salts of the 2,6-di(3-methylpyrazol-1-yl)pyrazine complex<sup>15a,c</sup> the amount of hydrogen bonding is reduced. Despite this reduced hydrogen bonding, both **4** and **5** show abrupt thermal spin transitions with narrow hysteresis loops, indicative of high levels of cooperativity. This observation suggests that it is the extensive network of  $\pi$  interactions in these structures which is responsible for the cooperative nature of the transitions. This hypothesis is further supported by the absence of these interactions in the 2,6-di(3-methylpyrazol-1-yl)pyrazine complexes in which the thermal spin transition is gradual and hydrogen bonding plays a critical role.

**6** crystallises in the tetragonal space group  $P\bar{4}2_1c$  with unit cell parameters of  $a = 9.587(1)$  Å,  $c = 17.933(4)$  Å and  $V = 1648.1(5)$  Å<sup>3</sup> at 250 K. The asymmetric unit consists of a quarter of the cation and one half of one anion, although at this temperature the anion is found to be disordered over the two fold axis, selected crystallographic parameters are presented in Table 3. The iron atom is situated on a four fold improper axis and, like all the compounds in this series, has a distorted octahedral geometry; bound equatorially to two ligands through three of their five nitrogen atoms, Fig. 5. The mean iron–nitrogen distance at this temperature is consistent with the compound being in the high-spin state. The iron atom lies on the origin with the iron–pyridine nitrogen (N3) bonds along the crystallographic  $c$  axis. Neighbouring iron atoms, therefore, are separated by a distance equal to the length of the  $c$  axis and are sited on a straight line through the unit cell.

**Fig. 5** Structure of the [Fe(L<sup>4</sup>)<sub>2</sub>]<sup>2+</sup> cation at 250 K in the HS-1 state. Hydrogen atoms have been omitted for clarity and thermal ellipsoids are at 50% probability.

Cooling to 30 K results in a crystallographic phase transition from  $P\bar{4}2_1c$  to the orthorhombic space group  $P2_12_12_1$  which involves a doubling of the crystallographic  $c$  axis. The asymmetric unit is one cation and two anions and there are four formula units in the unit cell. Neither independent anion is found to be disordered at this temperature. The mean iron–nitrogen distance of 1.947(9) Å, and the symmetry parameters, indicate that the iron(II) centre is in the low spin state, in agreement with the magnetic data. The loss of symmetry is caused by displacement of the cations such that the iron atoms are no longer aligned parallel to  $c$  but form a zigzag parallel to the  $c$  direction being displaced from each other in both the  $a$  and  $b$  directions and no longer being situated at the origin of the unit cell. This distortion of the packing prevents clashing of the methyl groups on contraction of the unit cell due to the spin transition. Monitoring the unit cell parameters with temperature demonstrates that the spin transition takes place abruptly between 240 K and 230 K. This is in good agreement with the results of magnetic experiments which estimate  $T_{1/2}$  as being 232 K.

Irradiation of the crystal on the diffractometer at 30 K with red laser light ( $\lambda = 632.8$  nm, 25 mW) results in a change in colour of the crystal from the dark yellow-brown associated with the low-spin state to the yellow of the high-spin state. However, on attempting to determine the unit cell parameters of the compound after irradiation, it was found that the crystal had been irreversibly damaged and the diffraction peaks had become very broad and diffuse.

In addition to the above behaviour, the photomagnetic studies on **6** described below showed a weak but consistent anomaly near 50 K, where a small fraction of the photoexcited sample undergoes LIESST relaxation at a lower temperature than the bulk. In the light of these results, a powder diffraction study of the same sample of **6** used for the photomagnetic study was carried out. It was found that, although the bulk of the sample was isostructural with the single crystal described above, it also contained *ca.* 10% of a second phase. The lower  $T$ (LIESST) shown by this contaminating phase suggests that it should undergo SCO at a substantially higher temperature than 232 K. While the diffraction peaks from this

contaminant were too weak to allow a unit cell to be refined, it is notable that crystals of the  $\text{BF}_4^-$  salt of the same complex molecule are low spin at 300 K. We therefore suggest that the minor phase of **6** is likely to be isostructural with  $[\text{Fe}(\text{L}^4)_2](\text{BF}_4)_2$  (**7**, ESI†). Be that as it may, the existence of a minor contaminant in bulk samples of **6** will not perturb the magnetic or photomagnetic behaviour of the major phase of this material.

### $T(\text{LIESST})$ database

We have now investigated the  $T(\text{LIESST})$  and  $T_{1/2}$  values of more than sixty iron(II) spin-crossover materials of nitrogen ligands, and have found their photomagnetic properties are governed by a simple linear relation (eqn (1)).<sup>7–9</sup> Four parallel  $T_0$  lines with values of 100, 120, 150 and 200 K have been defined so far, for different series of iron(II) compounds (Fig. 6). To solve the challenge of achieving room-temperature photo-bistability, we must now identify the factors controlling  $T_0$ , so that materials with higher  $T_0$  [and hence  $T(\text{LIESST})$ ] values can be designed.<sup>9</sup>

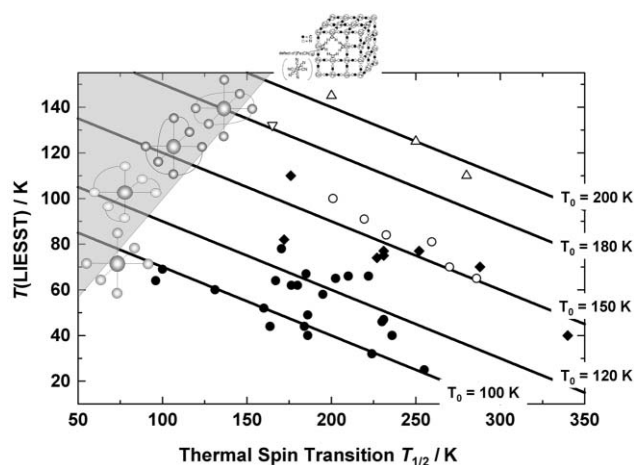


**Fig. 6** Variation of  $T(\text{LIESST})$  vs.  $T_{1/2}$  for **1–6** (○) in comparison with the literature data listed in ref. 9. The region in gray is meaningless as  $T(\text{LIESST})$  must be  $\leq T_{1/2}$ .

We have previously suggested that ligand denticity and flexibility, and the degree of distortion of the coordination sphere away from an ideal octahedral geometry, appear to be the most important factors in determining  $T_0$ .<sup>7–9</sup> In contrast, factors outside the inner metal coordination sphere (intermolecular cooperativity, crystal packing, identity of anions, solvent content) result in only small perturbations to  $T_0$ . The present work supports these suggestions, in that **1–6** lie very close together on the  $T_0 = 150$  K line in Fig. 6, that we have previously derived for a series of compounds  $[\text{Fe}(\text{bpp})_2]\text{X}_2 \cdot n\text{H}_2\text{O}$  ( $\text{bpp} = 2,6\text{-di}\{\text{pyrazol-3-yl}\}\text{pyridine}$ , a regioisomer of  $\text{L}^1$ ).<sup>8</sup> This is the first time that iron(II) complexes of two different series of ligands that are stereochemically similar, but otherwise distinct, have been shown to follow the same photomagnetic correlation. Both **1–6** and  $[\text{Fe}(\text{bpp})_2]\text{X}_2$  contain an iron(II) ion surrounded by six donor nitrogen atoms, contained in two ligands coordinated in the meridional planes of an (idealised) octahedron. The structural changes during SCO are very similar in the two series of compounds. Structure determinations of different members of the  $[\text{Fe}(\text{bpp})_2]\text{X}_2$  family<sup>25</sup> show that the average Fe–N distance is 1.95 Å in low-spin compounds,<sup>26,27</sup> and 2.16 Å in

high-spin structures.<sup>27,28</sup> These values are almost identical to those shown by **1–6**.<sup>13–16,25</sup> Hence, the two series undergo very similar structural changes during SCO, which causes an average change in Fe–N bond length of 0.21 Å. The “stiffness” of the ligand cage, and the twisting of the ligands around the metal ion during SCO, will also be very similar in the two series of compounds. So, from our previous arguments, despite their very different crystal chemistry it is reasonable that the light-generated metastable high-spin states of **1–6** and  $[\text{Fe}(\text{bpp})_2]\text{X}_2$  should show essentially identical thermal stability.

This discussion assumes that the structures of the thermal and photoinduced high-spin states of a given material are very similar. This hypothesis is certainly valid for **1**,<sup>14</sup> **4**<sup>16</sup> and **5** (this work) for which crystallographic data are available from the photoinduced HS form. The thermal high-spin state at 300 K, and the photo-induced high-spin state at 30 K, for all three compounds are isostructural. But this situation is less clear for the other members of the series, since **2**, **3**<sup>15</sup> and **6** (this work) all undergo crystallographic phase changes upon thermal SCO. In the absence of a structure determination it is uncertain whether photoexcitation of **2**, **3** or **6** also induces a crystallographic phase change. This would significantly affect the thermodynamics of their LIESST relaxation (Tables 1 and 2), although it would have only a small effect on their  $T_0$  parameters.<sup>9</sup>

## Conclusions

We have reported the thermal and photochemical spin-crossover properties of six iron(II) complexes based on the tridentate ligand. Although the structural chemistry of their spin transitions differs significantly between the compounds, they all obey the same linear  $T(\text{LIESST}) = T_0 - 0.3T_{1/2}$  law observed previously for a different family of iron(II) complex salts of a related tridentate ligand. These results emphasise the importance of the inner coordination sphere in controlling the lifetime of a photogenerated high-spin excited state in these materials.

We have also recorded the kinetics of the LIESST relaxation processes undergone by these compounds, and detected the existence of LITH hysteresis loops under constant irradiation. Both these studies indicate the importance of intermolecular cooperativity to the rate of relaxation of the LIESST metastable high-spin state in the solid. There is no obvious correlation between the parameters in Tables 1 and 2 and  $T_{1/2}$ , the width of the thermal spin transitions, or the structural chemistry of the spin transitions for **1–6** (e.g. whether or not they undergo a phase change during thermal SCO). This implies that other structural factors, that we cannot take account of, also contribute to the thermodynamics and kinetics of LIESST decay. These might include: changes in anion positions and/or motion; the onset of ligand conformational disorder (as observed in **4**<sup>16</sup> and **5** at 300 K, for example); or, more subtle differences in the geometries and strength of the interactions between spin centres in the high- and low-spin forms of the solids. Experiments designed to shed more light on this question are in progress.

## Experimental

Compounds  $[\text{Fe}(\text{L}^1)_2][\text{BF}_4]_2$  (**1**),<sup>10–12</sup>  $[\text{Fe}(\text{L}^2)_2][\text{BF}_4]_2$  (**2**) and  $[\text{Fe}(\text{L}^2)_2][\text{ClO}_4]_2$  (**3**),<sup>10,13</sup>  $[\text{Fe}(\text{L}^3)_2][\text{BF}_4]_2$  (**4**)<sup>14</sup> and  $\text{L}^3$ <sup>14</sup> were prepared

by the literature procedures. More detail about the crystal structure of **7** is given in the ESI.† Unless otherwise stated, all manipulations were carried out in air using reagent grade solvents, except that bis(2-methoxyethyl) ether was dried over sodium before use.

### Synthesis of 2,6-di{4-methylpyrazol-1-yl}pyridine (**L**<sup>4</sup>)

2,6-Dibromopyridine (1.3 g, 5.4 mmol) and potassium 4-methylpyrazolide [prepared *in situ* by treatment of 4-methylpyrazole (1.0 g, 12.2 mmol) with KH (0.49 g, 12.2 mmol)] were stirred in bis(2-methoxyethyl) ether (100 cm<sup>3</sup>) under N<sub>2</sub> at 130 °C for 5 days. Quenching the cooled reaction mixture with excess water yielded **L**<sup>4</sup> as a white solid which was used without further purification. Yield 0.58 g, 40%. Found C, 65.0; H, 5.5; N, 29.3%. Calcd for C<sub>13</sub>H<sub>13</sub>N<sub>5</sub>: C, 65.2; H, 5.5; N, 29.3%. Mp 121–123 °C. EI mass spectrum: *m/z* 240 [M + H]<sup>+</sup>. <sup>1</sup>H NMR (CDCl<sub>3</sub>): δ 2.16 (s, 6H, CH<sub>3</sub>), 7.56 (s, 2H, Pz H<sup>3</sup>), 7.74 (d, 2H, 7.5 Hz, Py H<sup>3/5</sup>), 7.86 (t, 1H, 7.5 Hz, Py H<sup>4</sup>), 8.29 (s, 2H, Pz H<sup>5</sup>). <sup>13</sup>C{<sup>1</sup>H} NMR (CDCl<sub>3</sub>): δ 8.9 (2C, CH<sub>3</sub>), 108.3 (2C, Py C<sup>3/5</sup>), 118.5 (2C, Pz C<sup>4</sup>), 125.4 (2C, Pz C<sup>5</sup>), 141.0 (1C, Py C<sup>4</sup>), 143.2 (2C, Pz C<sup>3</sup>), 150.0 (2C, Py C<sup>2/6</sup>).

### Synthesis of [Fe(L<sup>3</sup>)<sub>2</sub>][ClO<sub>4</sub>]<sub>2</sub> (**5**)

Treatment of Fe[ClO<sub>4</sub>]<sub>2</sub>·6H<sub>2</sub>O (0.15 g, 0.42 mmol) with **L**<sup>3</sup> (0.20 g, 0.84 mmol) in acetone (30 cm<sup>3</sup>) at room temperature yielded a yellow solution which was then filtered. Concentration of the solution to *ca.* 10 cm<sup>3</sup> yielded mustard yellow microcrystals, which were stored overnight at –30 °C, then isolated, washed with Et<sub>2</sub>O and dried *in vacuo*. Yield 0.18 g, 57%. Found C, 39.1; H, 3.0; N, 19.3%. Calcd for C<sub>24</sub>H<sub>22</sub>Cl<sub>2</sub>FeN<sub>10</sub>O<sub>10</sub>: C, 39.1; H, 3.0; N, 19.0%. ES mass spectrum: *m/z* 396 [<sup>56</sup>Fe(L<sup>3</sup>)(<sup>35</sup>ClO<sub>4</sub>)]<sup>+</sup>, 242 [L<sup>3</sup>H].

### Synthesis of [Fe(L<sup>4</sup>)<sub>2</sub>][ClO<sub>4</sub>]<sub>2</sub> (**6**)

Method as for **5**, using **L**<sup>4</sup> (0.20 g, 0.84 mmol). The brown acetone solution of the complex yielded mustard yellow microcrystals upon standing at –30 °C. Yield 0.31 g, 70%. Found C, 42.5; H, 3.6; N, 19.3%. Calcd for C<sub>26</sub>H<sub>26</sub>Cl<sub>2</sub>FeN<sub>10</sub>O<sub>8</sub>: C, 42.6; H, 3.6; N, 19.1%. ES mass spectrum: *m/z* 394 [<sup>56</sup>Fe(L<sup>4</sup>)(<sup>35</sup>ClO<sub>4</sub>)]<sup>+</sup>, 267 [<sup>56</sup>Fe(L<sup>4</sup>)<sub>2</sub>]<sup>2+</sup>.

### Synthesis of [Fe(L<sup>4</sup>)<sub>2</sub>][BF<sub>4</sub>]<sub>2</sub> (**7**)

Treatment of Fe[BF<sub>4</sub>]<sub>2</sub>·6H<sub>2</sub>O (0.14 g, 0.42 mmol) with **L**<sup>4</sup> (0.20 g, 0.84 mmol) in acetone (30 cm<sup>3</sup>) at room temperature yielded a brown solution which was then filtered. Concentration of the solution to *ca.* 10 cm<sup>3</sup> yielded brown microcrystals, which were stored overnight at –30 °C, then isolated, washed with Et<sub>2</sub>O and dried *in vacuo*. Yield 0.23 g, 78%. Found C, 44.0; H, 3.8; N, 19.9%. Calcd for C<sub>26</sub>H<sub>26</sub>B<sub>2</sub>F<sub>8</sub>FeN<sub>10</sub>: C, 44.1; H, 3.7; N, 19.8%. ES mass spectrum: *m/z* 621 [<sup>56</sup>Fe(L<sup>4</sup>)<sub>2</sub>(<sup>11</sup>BF<sub>4</sub>)]<sup>+</sup>, 553 [<sup>56</sup>Fe(L<sup>4</sup>)<sub>2</sub>F]<sup>+</sup>, 314 [<sup>56</sup>Fe(L<sup>4</sup>)F]<sup>+</sup>, 267 [<sup>56</sup>Fe(L<sup>4</sup>)<sub>2</sub>]<sup>2+</sup>. χ<sub>M</sub><sup>T</sup> (298 K) 0.090 cm<sup>3</sup> mol<sup>–1</sup> K.

[CAUTION: While we have experienced no difficulty in handling **5** and **6**, metal–organic perchlorates are potentially explosive and should be handled with due care in small quantities.]

### Magnetism and photomagnetism

The photomagnetic measurements were performed using a Spectrum Physics Series 2025 Kr<sup>+</sup> laser (λ = 532 nm) coupled *via* an optical fibre to the cavity of a MPMS-55 Quantum Design SQUID magnetometer. The optical power at the sample surface

was adjusted to 5 mW cm<sup>–2</sup>, and it was verified that this resulted in no change in magnetic response due to heating of the sample. Photomagnetic samples consisted of a thin layer of compound whose weight was obtained by comparison of the thermal spin crossover curve with that of a more accurately weighed sample of the same material. Our previously published standardised method for obtaining LIESST data was followed.<sup>11</sup> After cooling slowly to 10 K the sample, now in the low-spin state was irradiated and the change in magnetism followed. When the saturation point had been reached the laser was switched off and the temperature increased at a rate of 0.3 K min<sup>–1</sup>. The magnetisation was measured every 1 K. *T*(LIESST) was determined from the minimum of a dχ<sub>M</sub><sup>T</sup>/dT vs. *T* plot for the relaxation process.

### Crystallography

Single crystals of **5–7** were all grown by slow diffusion of Et<sub>2</sub>O vapour into MeNO<sub>2</sub> solutions of the compounds. Crystallographic data for **5** and **6** were collected on a Bruker SMART CCD<sup>29</sup> (ω-scan, 0.3° per frame) diffractometer using graphite-monochromated Mo-K<sub>α</sub> radiation (λ = 0.71073 Å). Between 360 K and 110 K the crystals were cooled in a flow of chilled nitrogen gas using an Oxford Cryosystems Cryostream.<sup>30</sup> Below this the crystals were cooled in a flow of chilled helium using an Oxford Cryosystems HELIX.<sup>31</sup> All data processing was carried out using the SAINT<sup>32</sup> and XPREP<sup>33</sup> software packages. Absorption corrections were applied using SADABS.<sup>33</sup> Data for **7** were collected using a Nonius KappaCCD diffractometer, with graphite-monochromated Mo-K<sub>α</sub> radiation, and fitted with an Oxford Cryosystems nitrogen-cooled low-temperature device. All data processing was carried out using DENZO<sup>34</sup> while an absorption correction was applied using SORTAV.<sup>35</sup> The structures were all solved by direct methods and refined on *F*<sup>2</sup> using full matrix least-squares methods within the SHELXTL suite. The hydrogen atoms were placed geometrically and treated with a riding model. For the LIESST experiments, the sample was irradiated for ten minutes whilst on the Bruker SMART diffractometer using a He–Ne laser (λ = 632.8 nm, 25 mW).

CCDC reference numbers 296687–296689 and 296691–296693.

For crystallographic data in CIF or other electronic format see DOI: 10.1039/b601366j

### Other measurements

Electron impact and electrospray (MeCN matrix) mass spectra were respectively performed with VG AutoSpec and Micromass LCT TOF spectrometers. CHN microanalyses were performed by the University of Leeds School of Chemistry microanalytical service. NMR spectra were run on a Bruker ARX250 spectrometer, operating at 250.1 MHz (<sup>1</sup>H) or 62.9 MHz (<sup>13</sup>C).

### Acknowledgements

The authors would like to thank Dr H. J. Blythe (University of Sheffield) for help with magnetic measurements, and C. A. Kilner (University of Leeds) for the crystal structure of **7**. Funding by the EPSRC for two studentships (V.A.M., J.E.) and a Senior Research Fellowship (J.A.K.H.), the Alliance bilateral action (J.-F.L, M.A.H.), the network of excellence MAGMANet

[FP6-515767-2] (J.-F.L.) and the Aquitaine Region (J.-F.L.) is gratefully acknowledged.

## References

- 1 See for general reviews: *Spin Crossover in Transition Metal Compounds, Topics in Current Chemistry*, ed. P. Gütllich and H. A. Goodwin, Springer Verlag, Vienna, 2004, vol. 233–235.
- 2 P. Gütllich, A. Hauser and H. Spiering, *Angew. Chem., Int. Ed. Engl.*, 1994, **33**, 1024.
- 3 A. Bousseksou, N. Negre, M. Goiran, L. Salmon, J.-P. Tuchagues, M.-L. Boillot, K. Boukheddaden and F. Varret, *Eur. Phys. J. B*, 2000, **13**, 451.
- 4 O. Kahn and C. J. Martinez, *Science*, 1998, **279**, 44; P. Gütllich, Y. Garcia and T. Woike, *Coord. Chem. Rev.*, 2001, **219–221**, 839; J.-F. Létard, P. Guionneau and L. Goux-Capes, *Top. Curr. Chem.*, 2004, **235**, 221.
- 5 D. R. Davydov, G. H. B. Hoa and J. A. Peterson, *Biochemistry*, 1999, **38**, 751; M. F. Perutz, G. Fermi, B. Luisi, B. Shannan and R. C. Liddington, *Acc. Chem. Res.*, 1987, **20**, 309; W. R. Schiedt and C. A. Reed, *Chem. Rev.*, 1981, **81**, 543; J. Badro, G. Fiquet, F. Guyot, J. P. Rueff, V. V. Struzhin, G. Vanko and G. Monaco, *Science*, 2003, **300**, 789.
- 6 J. J. McGarvey and I. Lawthers, *J. Chem. Soc., Chem. Commun.*, 1982, 906; S. Decurtins, P. Gütllich, C. P. Köhler, H. Spiering and A. Hauser, *Chem. Phys. Lett.*, 1984, **105**, 1.
- 7 J.-F. Létard, L. Capes, G. Chastanet, N. Moliner, S. Létard, J. A. Real and O. Kahn, *Chem. Phys. Lett.*, 1999, **313**, 115.
- 8 S. Marcen, L. Lecren, L. Capes, H. A. Goodwin and J.-F. Létard, *Chem. Phys. Lett.*, 2002, **358**, 87.
- 9 J.-F. Létard, P. Guionneau, O. Nguyen, J. S. Costa, S. Marcen, G. Chastanet, M. Marchivie and L. Capes, *Chem. Eur. J.*, 2005, **11**, 4582.
- 10 T. Buchen, P. Gütllich and H. A. Goodwin, *Inorg. Chem.*, 1994, **33**, 4573; T. Buchen, P. Gütllich, K. H. Sugiyarto and H. A. Goodwin, *Chem. Eur. J.*, 1996, **2**, 1134; C. H. Wu, J. Jung, P. K. Gantzel, P. Gütllich and D. N. Hendrickson, *Inorg. Chem.*, 1997, **36**, 5339; F. Renz, H. Oshio, V. Ksenofontov, M. Waldeck, H. Spiering and P. Gütllich, *Angew. Chem., Int. Ed.*, 2000, **39**, 699; S. Hayami, Z.-Z. Gu, Y. Einaga, Y. Kobayashi, Y. Ishikawa, Y. Yamada, A. Fujishima and O. Sato, *Inorg. Chem.*, 2001, **40**, 3240.
- 11 J.-F. Létard, P. Guionneau, L. Rabardel, J. A. K. Howard, A. E. Goeta, D. Chasseau and O. Kahn, *Inorg. Chem.*, 1998, **37**, 4432.
- 12 V. A. Money, J. S. Costa, S. Marcen, G. Chastanet, J. Elhaïk, M. A. Halcrow, J. A. K. Howard and J.-F. Létard, *Chem. Phys. Lett.*, 2004, **391**, 273.
- 13 J. M. Holland, J. A. McAllister, Z. Lu, C. A. Kilner, M. Thornton-Pett and M. A. Halcrow, *Chem. Commun.*, 2001, 577; J. M. Holland, J. A. McAllister, C. A. Kilner, M. Thornton-Pett, A. J. Bridgeman and M. A. Halcrow, *J. Chem. Soc., Dalton Trans.*, 2002, 548.
- 14 V. A. Money, I. Radosavljevic Evans, M. A. Halcrow, A. E. Goeta and J. A. K. Howard, *Chem. Commun.*, 2003, 158.
- 15 (a) J. Elhaïk, V. A. Money, S. A. Barrett, C. A. Kilner, I. Radosavljevic Evans and M. A. Halcrow, *Dalton Trans.*, 2003, 2053; (b) V. A. Money, I. Radosavljevic Evans, J. Elhaïk, M. A. Halcrow and J. A. K. Howard, *Acta Crystallogr., Sect. B*, 2004, **B60**, 41; (c) V. A. Money, J. Elhaïk, M. A. Halcrow and J. A. K. Howard, *Dalton Trans.*, 2004, 65.
- 16 V. A. Money, J. Elhaïk, M. A. Halcrow and J. A. K. Howard, *Dalton Trans.*, 2004, 1516.
- 17 D. L. Jameson and K. A. Goldsby, *J. Org. Chem.*, 1990, **55**, 4992.
- 18 F. Varret, M. Noguès and A. Goujon, *Photomagnetic properties of some inorganic solids*, ed. J. Miller and M. Drillon, Wiley VCH, Weinheim, Germany, 2002, vol. 2, p. 257.
- 19 J.-F. Létard, G. Chastanet, O. Nguyen, S. Marcen, M. Marchivie, P. Guionneau, D. Chasseau and P. Gütllich, *Monatsh. Chem.*, 2003, **134**, 165.
- 20 A. Hauser, *Coord. Chem. Rev.*, 1991, **111**, 275; A. Hauser, J. Jestic, H. Romstedt, R. Hinek and H. Spiering, *Coord. Chem. Rev.*, 1999, **190–192**, 471.
- 21 A. Hauser, J. Adler and P. Gütllich, *Chem. Phys. Lett.*, 1988, **152**, 468.
- 22 A. Desaix, O. Roubeau, J. Jestic, J. G. Haasnoot, K. Boukheddaden, E. Codjovi, J. Linarès, M. Nogues and F. Varret, *Eur. Phys. J. B*, 1998, **6**, 183.
- 23 P. Guionneau, C. Brigonteix, Y. Barrans, A. E. Goeta, J.-F. Létard, J. A. K. Howard, J. Gaultier and D. Chasseau, *C. R. Acad. Sci., Ser. IIc: Chim.*, 2001, **4**, 161; P. Guionneau, M. Marchivie, G. Bravic, J.-F. Létard and D. Chasseau, *J. Mater. Chem.*, 2002, **12**, 2546.
- 24 J. Kusz, H. Spiering and P. Gütllich, *J. Appl. Crystallogr.*, 2001, **34**, 229; M. Marchivie, P. Guionneau, J. A. K. Howard, G. Chastanet, J.-F. Létard, A. E. Goeta and D. Chasseau, *J. Am. Chem. Soc.*, 2002, **124**, 194; E. J. MacLean, C. M. McGrath, C. J. O'Connor, C. Sangregorio, J. M. W. Seddon, E. Sinn, F. E. Sowrey, S. J. Teat, A. E. Terry, G. B. M. Vaughan and N. A. Young, *Chem. Eur. J.*, 2003, **9**, 5314; A. L. Thompson, A. E. Goeta, J. A. Real, A. Galet and M. C. Muñoz, *Chem. Commun.*, 2004, 1390; J. Kusz, D. Schollmeyer, H. Spiering and P. Gütllich, *J. Appl. Crystallogr.*, 2005, **38**, 528.
- 25 M. A. Halcrow, *Coord. Chem. Rev.*, 2005, **249**, 2880.
- 26 H. Sugiyarto, D. C. Craig, A. D. Rae and H. A. Goodwin, *Aust. J. Chem.*, 1994, **47**, 869; K. H. Sugiyarto, K. Weitzner, D. C. Craig and H. A. Goodwin, *Aust. J. Chem.*, 1997, **50**, 869; E. Coronado, M. C. Giménez-López, C. Gimenez-Saiz, J. M. Martínez-Agudo and F. M. Romero, *Polyhedron*, 2003, **22**, 2375; M. L. Scudder, D. C. Craig and H. A. Goodwin, *CrystEngComm*, 2005, **7**, 642.
- 27 K. H. Sugiyarto, W.-A. McHale, D. C. Craig, A. D. Rae, M. L. Scudder and H. A. Goodwin, *Dalton Trans.*, 2003, 2443.
- 28 K. H. Sugiyarto, M. L. Scuddler, D. C. Craig and H. A. Goodwin, *Aust. J. Chem.*, 2000, **53**, 755.
- 29 *SMART-1000 CCD*, Bruker AXS, Madison, WI.
- 30 *Cryostream Cooler*, Oxford Cryosystems Ltd, Oxford, UK.
- 31 *Oxford Helix*, Oxford Cryosystems Ltd, Oxford, UK.
- 32 G. M. Sheldrick, *SHELXS-97, SHELXL 97. Program for the Refinement of Crystal Structures*, University of Göttingen, Germany, 1997.
- 33 G. M. Sheldrick, *SHELXTL Version 5.1. Bruker AXS*, Madison, WI, 1998.
- 34 Z. Otwinowski and W. Minor, *Methods Enzymol.*, 1997, **276**, 307.
- 35 R. H. Blessing, *Acta Crystallogr., Sect. A*, 1995, **51**, 33.